Conformation-driven strategy for resilient and functional protein materials

Xuan Mu[a,b] (ID), John S. K. Yuan Jr.[a] (ID), Jaewon Choi[a] (ID), Yixin Zhang[a], Peggy Cebe[c], Xiaocheng Jiang[a] (ID), Yu Shrike Zhang[b,1] (ID), and David L. Kaplan[a,1] (ID)

[a]Department of Biomedical Engineering, Tufts University, Medford, MA 02155; [b]Division of Engineering in Medicine, Department of Medicine, Brigham and Women's Hospital, Harvard Medical School, Cambridge, MA 02139; and [c]Department of Physics and Astronomy, Tufts University, Medford, MA 02155

The exceptional elastic resilience of some protein materials underlies essential biomechanical functions with broad interest in biomedical fields. However, molecular design of elastic resilience is restricted to amino acid sequences of a handful of naturally occurring resilient proteins such as resilin and elastin. Here, we exploit non-resilin/elastin sequences that adopt kinetically stabilized, random coil–dominated conformations to achieve near-perfect resilience comparable with that of resilin and elastin. We also show a direct correlation between resilience and Raman-characterized protein conformations. Furthermore, we demonstrate that metastable conformation of proteins enables the construction of mechanically graded protein materials that exhibit spatially controlled conformations and resilience. These results offer insights into molecular mechanisms of protein elastomers and outline a general conformation-driven strategy for developing resilient and functional protein materials.

elasticity | polymorphism | silk | conformation | protein

Resilient protein materials play essential biomechanical roles, including locomotion of insects and the reversible deformation of the aorta, skin, and lung alveoli (1, 2); they are also promising structural materials for a spectrum of biomedical applications such as tissue regeneration (3, 4), wearable bioelectronics (5, 6), and soft robotics/machines (7–9). Resilience is a crucial aspect of material elasticity that indicates the efficient energy transduction in cyclic deformations in contrast to energy dissipation (*SI Appendix*, Fig. S1) (2, 10). Traditionally, the molecular design of protein elastomers is mainly derived from naturally occurring primary sequences of highly resilient proteins such as resilin and elastin (*SI Appendix*, Tables S1 and S2) (11–13). However, these naturally occurring sequences only occupy a minute portion of the sequence space that consists of all combinations of the 20 amino acids (14), suggesting the potential for a large number of unexploited design opportunities. Also, in contrast to de novo systems (15, 16), naturally occurring sequences often lack programmable properties and functional tunability. Thus, the narrow scope of naturally occurring resilient proteins restricts the potential utility of resilient protein materials.

It is a challenge to exploit non-resilin/elastin sequences for developing resilient proteins. Most recombinant protein materials with modular-designed sequences, such as elastin-like proteins (ELP) and silk–elastin-like proteins (SELP), are useful to generate new elastic properties but largely rely on the native motifs (12). The high resilience of globular and de novo–designed protein elastomers, including bovine serum albumin (17) and ferredoxin-like proteins (18), are restricted by strong denaturants such as 6 M guanidinium chloride. Silk fibroin, regenerated from the silk cocoons of domesticated *Bombyx mori*, has been formed into tunable elastomers (*SI Appendix*, Table S3) (19, 20), yet the molecular origin of the elasticity remains largely untested.

According to sequence–conformation–property relationships, protein conformation is tightly associated with the mechanical

property of protein materials. Protein conformations have been exploited for advanced fabrication (21), tunable modulus and strength for individual materials (22, 23), responsive materials (24, 25), and shape-memory materials (26, 27). Resilient proteins tend to form random coil–dominated conformations characterized by the flexible interchange between a variety of spatial arrangements of polypeptide chains (2, 28). The random coils give rise to considerable conformational entropy and, in turn, entropy elasticity, analogous to rubber elasticity (Fig. 1C and *SI Appendix*, Fig. S3) (10, 29). There are a large number of proteins and domains exhibiting intrinsically disordered conformations or random coils (30). However, it remains largely unexploited whether non-resilin/elastin sequences can realize the exceptional resilience of resilin and elastin (11, 31). Here, we propose to exploit the random coil–dominated conformations derived from non-resilin/elastin sequences for highly resilient and elastically graded protein materials.

Results and Discussion

We exploited the metastable random coils of regenerated silk fibroin to prove the concept of the proposed conformation-driven strategy (Fig. 1A and *SI Appendix*, Fig. S2). Before

Significance

We provide insights into the sequence–conformation–property relationship that is central to the mechanical properties of protein elastomers. We find that a high content of glycine residue alone, not including proline, is sufficient for achieving near-perfect resilience. The content of proline residue may be associated with the metastability of random coils. Also, Raman spectroscopy, as a potent tool for investigating the conformation–property relationship, gives rise to a direct correlation between semiquantitative Raman features and the magnitude of elastic resilience. Moreover, metastable conformation or conformational polymorphism is useful to develop continuously and mechanically graded protein materials that may exhibit unique structural merits. This work underlies the exploitation of natural and de novo–designed sequences for protein elastomers and materials.
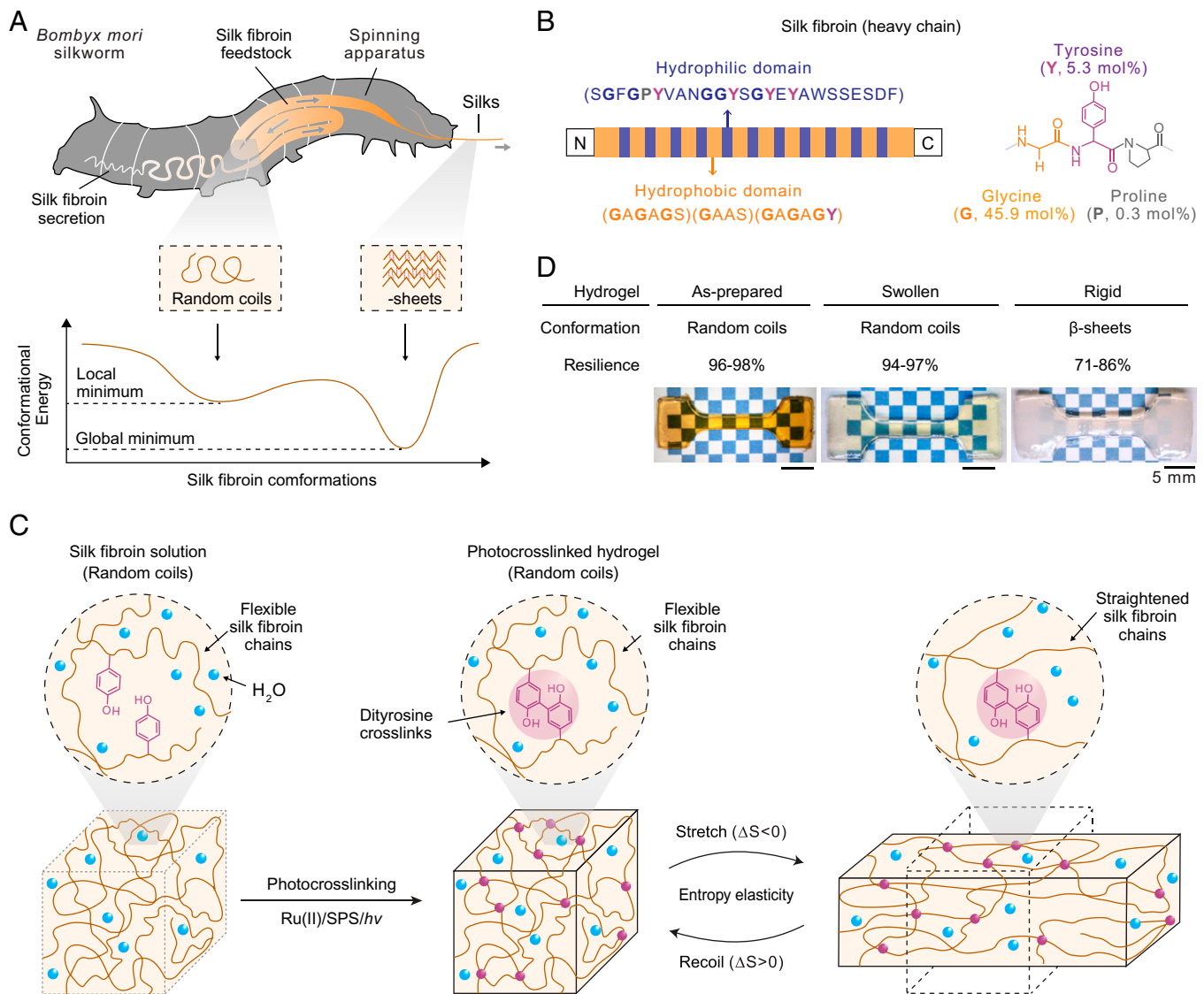
ENGINEERING

BIOCHEMISTRY

Fig. 1. Design and fabrication of resilient protein hydrogels by exploiting metastable random coils of silk fibroin. (*A*) Illustration of conformational change of silk fibroin from random coils to β-sheets. Silk fibroin is the primary structural component of *B. mori* silkworm silks. A hypothetical energy landscape of silk fibroin implies metastable random coils with a shallower and broader energy funnel and a local energy minimum, and stable β-sheets with a deeper and narrower funnel and a global energy minimum. Arrows indicate flow direction of silk fibroin feedstock. (*B*) Illustration of molecular designs of silk fibroin (heavy chain, molecular weight around 390 kDa) that consists of N and carboxyl termini and alternately positioned 12 hydrophobic and 11 hydrophilic domains. Characteristic motif sequences are shown in brackets. It contains 45.9 mol% G, 5.3 mol% Y, and 0.3 mol% P. (*C*) Schematics of the photo-crosslinking of regenerated silk fibroin solutions into hydrogels using Tris(2,2'-bipyridyl) ruthenium [Ru(II)], SPS, and white light (*hν*). Tyrosine residues are photo-oxidized to form di- or trityrosine crosslinks. Random coil-dominated conformation is a prerequisite for entropy elasticity. The stretching under external force leads to straightened molecular chains and decreased conformational entropy ($\Delta S < 0$); upon removing external force, entropy spontaneously increases ($\Delta S > 0$), which drives molecular recoil without energy loss or dissipation (i.e., high resilience). We used birefringence to probe stretched and recoiled silk fibroin molecules in *SI Appendix*, Fig. S3. (*D*) The set of as-prepared, swollen, and rigid silk fibroin hydrogels with distinct properties provide a comparative basis for investigating conformation-based resilience. Hydrogel fabrication is illustrated in *SI Appendix*, Fig. S2A.

spinning, silk fibroin adopts predominantly random coils in native silk feedstocks because random coils help prevent premature protein aggregation during in vivo storage of the silk feedstock over weeks. After silk spinning, the predominant conformation of silk fibroin transforms from random coils to β-sheets (Fig. 1*A* and *SI Appendix*, Fig. S2) (32, 33). The (meta)stability of silk fibroin conformations can be explained by the theory of the energy landscape (34, 35), in which metastable random coils are assumed to be kinetically stabilized in a local energy minimum, in contrast to the stable β-sheets exhibiting the lowest global energy (Fig. 1*A*). Accordingly, the random coil to β-sheet transition is largely inevitable for silk fibroin,

unlike naturally occurring resilient proteins that adopt stable random coil structures (2, 28). Notably, the conformational transition of silk fibroin can be impeded and accelerated by hyaluronic acid (20) and methanol (36), respectively, as examples of many options (23, 32). The kinetical control of conformations is likely based on tuning energy barriers or pathways between local and global minima.

The characteristic sequences of silk fibroin are associated with the metastable conformation and material properties such as resilience and hydrogel hydration. Silk fibroin (heavy chain) is composed of alternately positioned hydrophilic and hydrophobic domains (Fig. 1*B*). The hydrophilic domains contain

hydrophilic and negatively charged amino acids, such as aspartic acid (D), glutamic acid (E), and serine (S), as well as a characteristic 25-residue sequence motif, SGFGPYVANGGYSGYEYAWS-SESDF. The hydrophobic domain contains primarily glycine (G), alanine (A), and S, as well as motifs, such as GAGAS and GAAS. Notably, hydrophobic domains contain no charged residues. Thus, the hydration of silk fibroin hydrogels is primarily attributed to hydrophilic domains. In addition, the motif GAGAS in the hydrophobic domain can adopt either random coils or β-sheets, allowing the metastable conformation of silk fibroin. In contrast, the hydrophilic domain lacks specific motifs for regular secondary structure and thus largely remains as random coils.

Comparing amino acids between silk fibroin and naturally occurring resilient proteins provides insights into the molecular mechanism of resilience. The G content of silk fibroin is around 45.9 mol%, which is comparable to other resilient proteins such as aortic elastin (30 mol%) and insect resilin (39 to 42 mol%) (*SI Appendix*, Table S1). G is hydrophobic and has the smallest side chain, a hydrogen atom, thus benefiting chain flexibility and entropy elasticity of protein materials (10, 37). In addition, the proline content of silk fibroin (P, 0.3 mol%) is much lower than that found in naturally occurring resilient proteins such as elastin (P, 12 mol%) and resilin (P, 7 to 12 mol%) (*SI Appendix*, Table S1) (38). Proline has a unique five-member ring with restricted backbone conformations and has been known to resist the formation of β-sheets (38). The low proline content of silk fibroin may explain, in part, the capability to form β-sheets. Thus, we suggested that a high glycine content seems sufficient for the exceptional resilience and that the low proline content would not compromise the magnitude of the elastic resilience but seems associated with the metastable random coil conformation.

We cross-linked regenerated silk fibroin in solution to form hydrogels via a ruthenium [Ru(II)]/persulfate–mediated approach that is based on the photo-oxidation and coupling of tyrosine residues (39–41) (Fig. 1*C*). The dynamic photo–cross-linking process was investigated by three measurements: dityrosine fluorescence, damping factor [tan(δ)], and water content (Fig. 2 *A* and *D* and *SI Appendix*, Figs. S4–S6 and *Supplementary Text*). We also investigated cell encapsulation and in vitro degradation to imply the biomedical potential of photo–cross-linked silk fibroin hydrogels (*SI Appendix*, Fig. S7 and *Supplementary Text*). C3H/10T1/2s cells, encapsulated in the silk fibroin hydrogels, exhibited cytoskeleton development and considerable viability and metabolic activity.

We prepared a set of silk fibroin hydrogels with distinct conformations and mechanical properties, including "as-prepared," "swollen," and "rigid," which provides insights into the conformation-based resilience on a comparative basis (Fig. 1*D*). The silk hydrogel, after photo–cross-linking, is termed as-prepared. It is not treated with solvents for swelling, thus maintaining the same water content and chemical composition (including unreacted cross-linking reagents) as the photo–cross-linking precursor solution. The "swollen hydrogel is obtained by incubating as-prepared ones in 0.9 wt/vol% sodium chloride for 3 d (*SI Appendix*, Figs. S2 and S6). The incubation swells the hydrogel and washes away the unreacted reagents and polypeptide chains. As a result, water content increases from 75% (as-prepared) to over 85% (swollen) (*SI Appendix*, Fig. S6); the color of the silk hydrogel changes from orange (as-prepared) to light yellow (swollen) due to the removal of colored reagents such as Ru(II) (*SI Appendix*, Fig. S6). The aqueous solution of 25 wt% silk fibroin is also in light yellow. The rigid hydrogel is obtained by incubating swollen ones in 90 vol/vol% methanol for 1 h, transforming random coils into β-sheets (*SI Appendix*, Fig. S2). The name "rigid" is coined out of the mechanical property; the rigid hydrogel exhibits an increased Young's modulus and decreased resilience compared to the other two hydrogels (Fig. 1*D* and *SI Appendix*, Fig. S9).

The rigid hydrogel is immersed in 1× phosphate-buffered saline (PBS) and remains hydrated throughout this work.

Raman and Fourier-transform infrared (FTIR) spectroscopies were utilized to characterize the conformation of silk fibroin materials (Fig. 2 and *SI Appendix*, Fig. S8). The conformation-specific results of both Raman and FITR spectra have been verified by nuclear magnetic resonance (NMR), circular dichroism, and wide/small-angle X-ray scattering (WAXS/SAXS) (29, 42). Suggested by the spectral results, silk fibroin solution, as-prepared, and swollen hydrogels were dominated by random coils, in contrast to β-sheet–dominated rigid hydrogels (Fig. 2 and *SI Appendix*, Fig. S8 and *Supplementary Text*). Random coil–related characteristics of Raman spectra include amide I band (C = O stretching) at 1,667 cm^{-1}, tyrosine doublet at 850 cm^{-1} and 830 cm^{-1} (Tyr), amide III band (mainly C-N stretching) at 1,251 cm^{-1}, and two backbone stretching vibrations (C-C) at 1,103 cm^{-1} and 942 cm^{-1} (43, 44). In particular, the full width at half maximum (FWHM) of Raman amide I and the Raman Tyr ratio (I_{850}/I_{830}) were used for semiquantitative comparisons of protein conformations (42, 45). For solutions and as-prepared and swollen hydrogels, the FWHM of amide I and the Tyr ratio remained around 59 cm^{-1} and above 3, respectively, suggesting that random coil–dominated conformations largely remained after cross-linking and swelling (Fig. 2 *D–F* and *SI Appendix*, Fig. S8). The dityrosine crosslink likely restricts the vibration of tyrosine phenol rings, thus resulting in the decreased Raman Tyr ratio from 3.6 ± 0.1 to 3.3 ± 0.2; the swelling of the molecular networks may facilitate the ring vibration, increasing the Tyr ratio to 4.1 ± 0.6.

We also used deconvoluted FTIR spectra (46) to corroborate the random coil–dominated conformations of silk fibroin solutions and swollen hydrogels (Fig. 2 *C* and *G*). The solution and the swollen hydrogel exhibit the FTIR amide I band at 1,647 cm^{-1} and 1,645 cm^{-1}, respectively, indicating random coil dominance. In contrast, the FTIR amide I of the rigid hydrogel at 1,621 cm^{-1} indicates β-sheet dominance. Also, FTIR deconvolution estimated the random coil content of the solution and the swollen hydrogel, which is 78 ± 5% and 77 ± 7%, respectively, compared with the low content of β-sheets (2%), thus verifying the random coil dominance (Fig. 2*G*). Notably, several protein hydrogels exhibited conformational changes after cross-linking, such as enzyme–cross-linked silk fibroin elastomers (19). The improvement in the current work may be attributed to the short cross-linking time of the Ru(II)/persulfate approach (2 to 3 min) compared with that of the enzymatic approach (30 to 60 min); short cross-linking time minimizes the disturbance to the initial conformation (39, 40). The random coil–dominated conformation is a prerequisite for the entropy elasticity of protein hydrogels.

We employed uniaxial tensile tests and dynamic mechanical analysis (DMA) to characterize the elastic resilience of the three silk fibroin hydrogels, including as-prepared, swollen, and rigid (Fig. 3, *SI Appendix*, Figs. S9–S11, and Movie S1). At 0.1 mm/mm tensile strain, as-prepared and swollen hydrogels exhibited near-perfect resilience of 98.2 ± 0.7% and 97.3 ± 1. 3%, respectively, in contrast to rigid hydrogels with a relatively low resilience of 86.2 ± 0.9% (Fig. 3 *B* and *C* and *SI Appendix*, Fig. S9). The resilience of as-prepared hydrogels remained stable at 96.8 ± 1.1% with increased tensile strains from 0.1 mm/mm to 0.9 mm/mm (Fig. 3 *B* and *C*) and at 97.5 ± 0.5% with 20 consecutive stretch–recoil cycles and 0.5 mm/mm strain (*SI Appendix*, Fig. S9). Swollen hydrogels maintained largely above 95% resilience at increased tensile strains up to 0.6 mm/mm (Fig. 3*C* and *SI Appendix*, Fig. S9). In contrast, the resilience of rigid hydrogels exhibited a significant reduction from 86.2 ± 0.9% at 0.1 mm/mm to 70.8 ± 4.4% at 0.2 mm/mm (*SI Appendix*, Fig. S9). Similarly, a globular protein-based elastomer (GRG$_5$RG$_4$R) exhibited a drastic strain-dependent decrease in resilience from near 100% at 0.1

Mu et al.
Conformation-driven strategy for resilient and functional protein materials

PNAS | 3 of 8
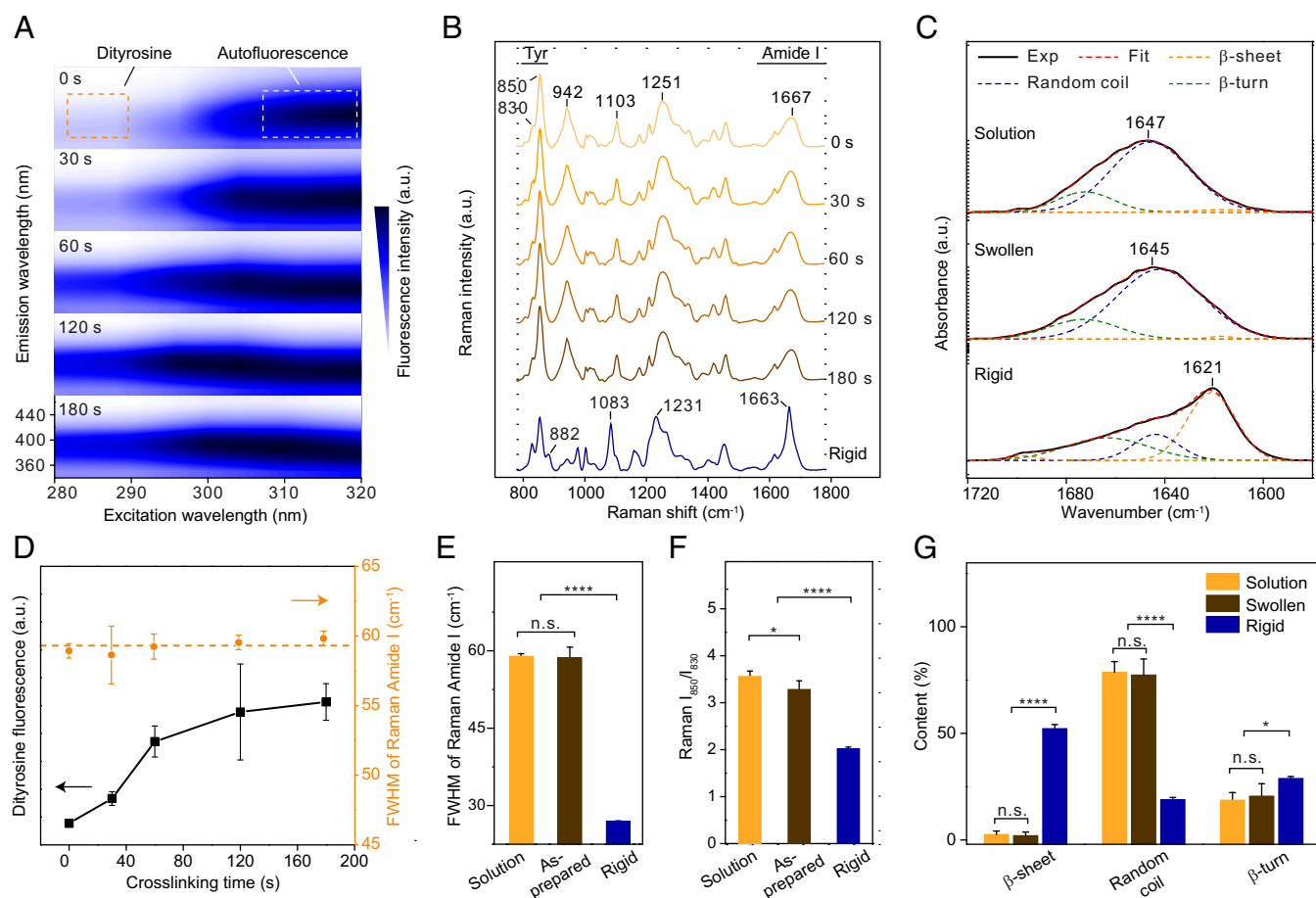https://doi.org/10.1073/pnas.2115523119

Fig. 2. Conformational characterizations of silk fibroin materials. (*A*) Fluorescence excitation-emission matrix spectra at crosslinking times from 0 to 180 s. Characteristic fluorescence of dityrosine crosslinks and autofluorescence of silk fibroin and Ru(II) are indicated. (*B*) Raman spectra at crosslinking times from 0 to 180 s, compared with rigid hydrogels. Two regions, including amide I band (at around 1,667 cm^{-1}) and tyrosine doublet (Tyr, at 850 and 830 cm^{-1}), are labeled. (*C*) FTIR amide I band of silk fibroin solutions, swollen, and rigid hydrogels. Deconvolution of the FTIR amide I band gives rise to semiquantitative content of three major conformations/secondary structures of silk fibroin, including random coils, β-sheets, and β-turns. (*D*) Random coil–dominated conformations remained after photo–cross-linking, as evidenced by dityrosine fluorescence and FWHM of Raman amide I band. (*E* and *F*) FWHM of Raman amide I band and Tyr ratio (I$_{850}$/I$_{830}$) of silk fibroin solutions, as-prepared, and rigid hydrogels. (*G*) Conformation content estimated by deconvoluted FTIR amide I band. (*n* = 3 independent spectra, ****P < 0.0001, *P < 0.1, n.s. P > 0.1, single-factor ANOVA followed by Scheffé's post hoc test).

mm/mm to around 76% at 0.9 mm/mm (4). The reduced resilience was due to the energy-dissipated unfolding of force-resistant globular domains (4) and β-sheets (35). In addition, DMA results verified the exceptional resilience of as-prepared and swollen hydrogels, which, at 1 Hz, are 95% and 91%, respectively (Fig. 3*E* and *SI Appendix*, Fig. S10). In contrast, the resilience of rigid hydrogels is 77% at 1 Hz. We also discussed other mechanical differences between silk fibroin hydrogels, associated with the swelling of the molecular network and the conformational transformation, in *SI Appendix, Supplementary Text*.

The resilience of as-prepared and swollen silk fibroin hydrogels was superior to or comparable with the most resilient protein elastomers known, including dragonfly tendon resilin (92%), bovine ligament elastin (90%), tendon collagen (90%), abductin (96%), recombinant resilin/resilin-like proteins (up to 97%), ELP (up to 84%), and methacryloyl-modified tropoelastin (76%) (Fig. 3*D* and *SI Appendix*, Table S2). Also, the DMA-characterized resilience of as-prepared and swollen silk fibroin hydrogels was almost coincident with resilin and elastin in the overlapped range of frequency roughly from 1 to 10 Hz (Fig. 3*E*). The resilience of as-prepared and swollen hydrogels was also superior to natural silk materials (around 30%) and

other silk fibroin hydrogels (up to 94.6% by compression tests) (*SI Appendix*, Tables S2 and S3). The improved resilience was primarily due to the well-maintained predominance of random coils, in contrast to β-sheet dominance of natural silk materials (Fig. 1*A*) (32, 35). These results highlighted the feasibility of random coil–forming non-resilin/elastin sequences, such as that of silk fibroin, to achieve the resilience as exceptional as that of resilin and elastin, thus providing avenues for developing resilient protein materials.

We examined the conformational origin of the elastic resilience of silk fibroin hydrogels by fitting the tensile stress–strain curves with the statistical rubber theory (Fig. 3*B* and *SI Appendix*, Fig. S9) (10). The as-prepared and swollen hydrogels agreed well with the statistical rubber theory below 0.5 and 0.3 mm/mm strains, respectively, verifying the rubber-like/random coil nature of as-prepared and swollen hydrogels. Notably, the fitting range was wider than the 0.25-mm/mm strain of a recombinant resilin protein (13). We ascribed this difference to the higher molecular weight of the regenerated silk fibroin (around 100 kDa) than the resilin protein (28.5 kDa), because longer molecular chains may lead to more random links, thus better fitting the Gaussian assumption of the rubber network theory
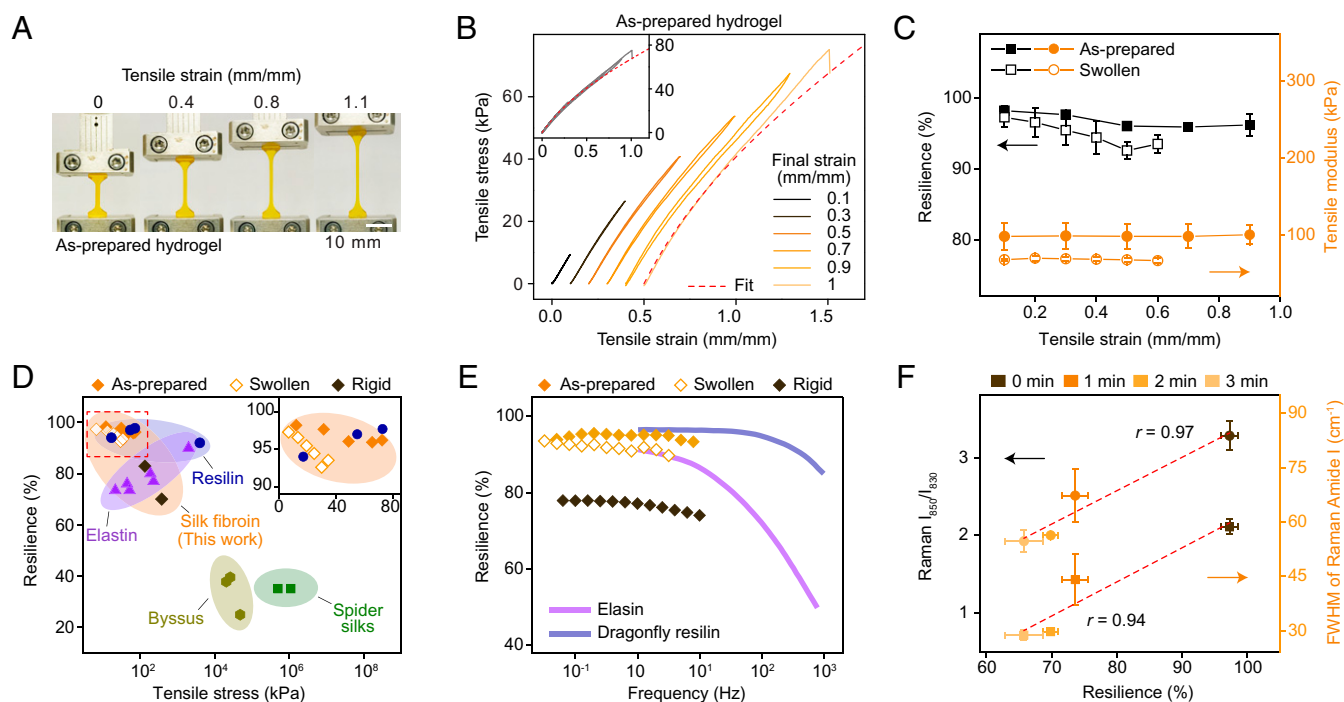
Fig. 3. Mechanical characterizations of silk fibroin hydrogels. (*A*) Optical images of as-prepared hydrogels stretched over 1 mm/mm strain in uniaxial tensile tests. (*B*) Consecutive cyclic tensile tests of as-prepared hydrogels with increased final strains from 0.1 to 1 mm/mm. The curves are shifted along the x-axis for clarity. *Inset* shows superimposable curves, indicating hydrogel recoverability. Red dashed curves indicate fitting results with statistical rubber theory and begin to deviate roughly at 0.5 mm/mm strain. (*C*) Resilience and tensile modulus of both as-prepared and swollen hydrogels as a function of final strains. (*D*) Comparison of silk fibroin hydrogels to other resilient protein materials in terms of resilience and tensile stress, also provided in *SI Appendix*, Table S2. *Inset* highlights data points within the red dashed box. (*E*) Resilience of silk fibroin hydrogels tested by DMA, in comparison to replotted data of resilin and elastin from ref. 10. (*F*) Direct correlation between elastic resilience and conformation-specific Raman features, including Raman Tyr ratio (I_{850}/I_{830}) and FWHM of the Raman amide I band. Methanol treatment from 0 to 3 min was used to induce incremental change of conformations and mechanical properties. Red dashed lines indicate linear regressions with corresponding Pearson's correlation coefficients, *r*.

(10). Also, the higher molecular weight may be advantageous for ultimate tensile strength and extensibility (*SI Appendix*, Table S2 and *Supplementary Text*).

Another notable finding of this study is the direct correlation between elastic resilience and Raman-characterized conformations, supplementing conventional conformation–property relationships of protein materials. We treated swollen silk fibroin hydrogels with 90 vol/vol% methanol for 0, 1, 2, or 3 min (Fig. 3*F* and *SI Appendix*, Fig. S11). With increased treatment times, the Raman Tyr ratio and the FWHM of Raman amide I decreased from 3.3 ± 0.2 to 1.9 ± 0.1 and from 58.6 ± 2.1 cm^{-1} to 28.7 ± 1.4 cm^{-1}, respectively, implying the incremental transition from random coils to β-sheets. Also, the resilience decreased from $97.3 \pm 1.3\%$ to $65.7 \pm 2.9\%$, and Young's modulus increased from 67.7 ± 1.6 kPa to 1.2 ± 0.4 MPa (Fig. 2*B* and *SI Appendix*, Fig. S9). Furthermore, the elastic resilience was directly correlated to the Raman Tyr ratio and the FWHM with Pearson's correlation coefficients of 0.97 and 0.94, respectively (Fig. 3*F*). These results indicated an early part of the transforming process from swollen to rigid hydrogels, supported the conformational origin of the elastic resilience, and suggested the potential to modulate resilience via tuning conformations. Also, due to the direct correlation, Raman spectroscopy may be a promising tool for exploring conformation-based elasticity.

We further exploited the conformation-driven strategy and the metastable random coils of silk fibroin to construct mechanically graded protein materials (Fig. 4 and *SI Appendix*, Figs. S12–S15). Protein conformations have been used to tune the modulus and strength of individual materials (22, 23) yet failed to produce continuously graded materials that are ubiquitous in living organisms (35, 47) and allow unique structural merits

(48). Also, protein conformation may be a viable alternative to the material composition found in naturally occurring graded protein tissues (35, 47) (*SI Appendix*, Table S4) for making graded materials. Protein conformation can be dynamically controlled (24, 25) and thus leads to a dynamic mechanical gradient.

We developed a directional methanol-treatment method to realize the spatial gradient of protein conformation (Fig. 4 and *SI Appendix*, Fig. S12 and *Supplementary Text*). Raman characterization suggested random coil–dominated and β-sheet–dominated conformations at the two ends of graded hydrogels, respectively (*SI Appendix*, Fig. S13). In the middle transition region, the FWHM of Raman amide I and the Raman Tyr ratio spatially changed from 55 cm^{-1} to 28 cm^{-1} and from 3.8 to 2.4, respectively, implying a continuous spatial transformation from random coils to β-sheets (Fig. 4*C* and *SI Appendix*, Fig. S13). Also, we used cyclic compression tests to characterize the local mechanical properties of graded hydrogels (Fig. 4*D* and *SI Appendix*, Fig. S14). The resilient end of the graded hydrogel exhibited 55.5 ± 1.5 kPa modulus and $92.8 \pm 3.4\%$ resilience; the rigid end exhibited 732.1 ± 19.5 kPa and $53.6 \pm 1.2\%$; and the transition zone exhibited 149.1 ± 11.7 kPa and $68.9 \pm 4.1\%$ in the middle between that of the two ends due to the transitioning nature. Furthermore, we developed a finite element-based model of the graded silk fibroin hydrogels, based on the actual size and the experimentally obtained moduli (Fig. 4*E* and *SI Appendix*, Fig. S15). Simulation results of graded hydrogels with 180° rotation agreed well with experimental results, including the rotated shape and the spiral position. These results corroborated the graded silk fibroin hydrogels with both conformational and mechanical gradients and verified the conformation-driven strategy for making graded protein material.
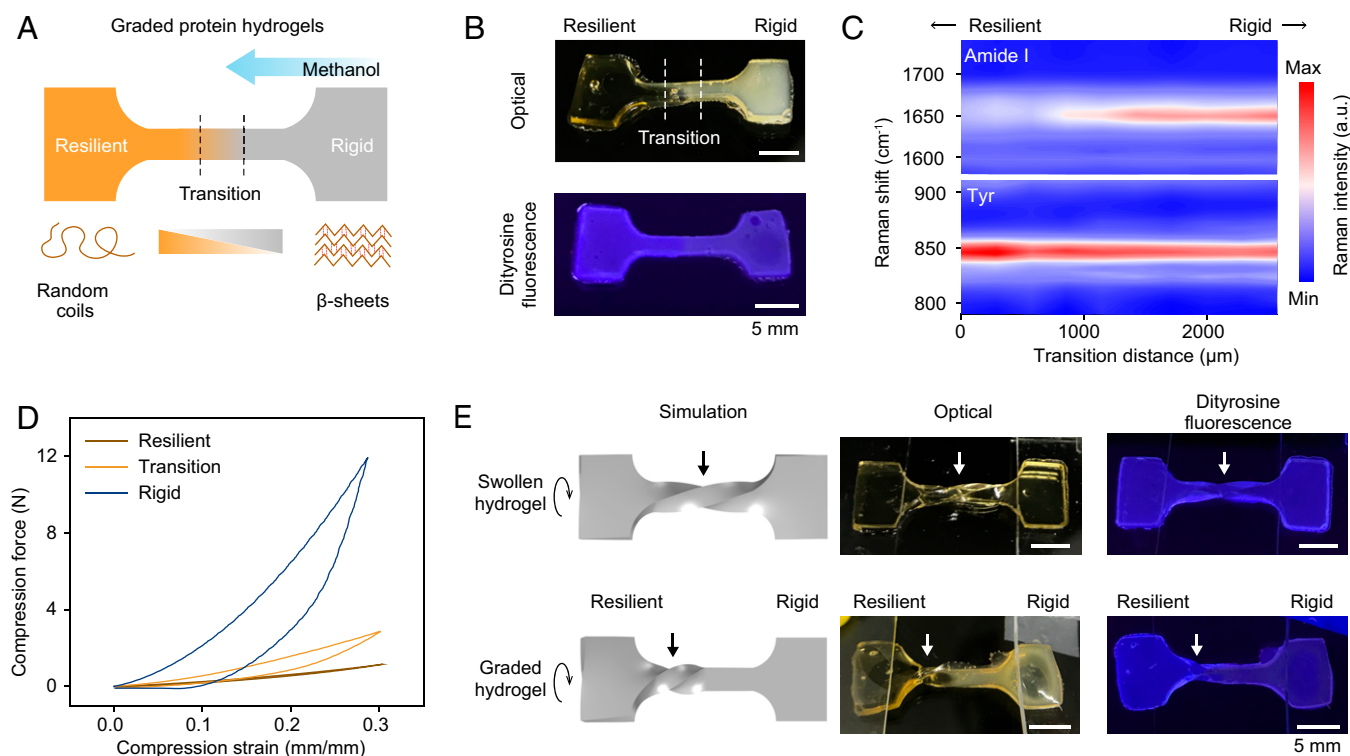
Mu et al.
Conformation-driven strategy for resilient and functional protein materials

PNAS | 5 of 8
https://doi.org/10.1073/pnas.2115523119

ENGINEERING

BIOCHEMISTRY

Fig. 4. Graded protein materials. (*A*) Schematics of directional methanol treatment and resultant graded silk hydrogels with spatially controlled conformations and mechanical properties. Graded hydrogels are roughly composed of a resilient end, a rigid end, and a middle transition zone. (*B*) Optical and fluorescent images of graded hydrogels. Blue fluorescence at 300 nm excitation is the characteristic of dityrosine cross-links. (*C*) Mapping spectra of Raman amide I band and Raman tyrosine doublet (Tyr, at 850 cm^{-1} and 830 cm^{-1}) over around 2.5 mm in the transition region. Arrows indicate the direction of resilient and rigid ends. (*D*) Typical cyclic compression curves of cylindrical samples punched out from local regions of graded hydrogels. (*E*) Simulated and experimental results of swollen and graded silk hydrogels after 180° rotation. Straight arrows indicate the center of rotating spirals. The ends of graded hydrogels are fixed under glass slides.

In conclusion, we exploited protein conformation of non–resilin/elastin sequences to construct exceptionally resilient and graded protein hydrogels. The direct correlation between conformation-related Raman features and elastic resilience provides a semiquantitative tool to probe the molecular mechanism of protein elastomers. The conformation-driven strategy would be generally useful for exploiting naturally occurring sequences and de novo–designed variants to develop a range of elastic protein biomaterials.

Materials and Methods

Regeneration of Silk Fibroin Solutions. Silk fibroin was regenerated from the cocoons of domesticated *B. mori* silkworms (Tajima Shoji Co.) as previously described (33). Briefly, 10 g sliced silkworm cocoons were degummed by boiling in 4 L 0.02 M sodium carbonate solution (S7795, Sigma-Aldrich) for 30 min, dried overnight in chemical hoods, and solubilized in 9.3 M lithium bromide solution (213225, Sigma-Aldrich) at 60 °C for 4 h, followed by dialyzing molecular weight cut-off (MWCO), 3,500) against deionized (DI) water with six changes of water over 3 d. The insoluble particulates were removed by centrifugation (two times at 9,000 rpm, 20 min, 4 °C) and sterile cell strainers (70-μm pore size, Fisherbrand, Fisher Scientific). The mass concentration of silk fibroin solutions was determined as the ratio of wet weight to dry weight (around 8 wt%). The molecular weight of the regenerated silk fibroin is subject to the degumming and dissolving conditions (32, 49), and in the current work, it was estimated to span a broad distribution with a center at around 100 kDa, according to previous results (50). The silk fibroin solutions were enriched to around 27 wt% by air-drying in Slide-a-Lyzer dialysis cassettes (MWCO 3,500 Da, Thermo Fisher Scientific) at 4 °C for 7 d. The regenerated silk fibroin solutions were yellowish clear and were stable at 4 °C for at least 4 wk.

Fabrications of Silk Fibroin Hydrogels. Silk fibroin solutions were mixed with 20 mM sodium persulfate (SPS, S6172, Sigma-Aldrich) and 2 mM

Tris(2,2′-bipyridyl) dichlororuthenium (II) hexahydrate [Ru(II), 544981, Sigma-Aldrich] to prepare photo–cross-linking precursor solutions unless otherwise noted. The light source for the photo–cross-linking was a 7-W (525 lm) light-emitting diode (LED) task lamp (3001, Electrix). The light illuminance (lux) was measured by an LED light meter (LT40, Extech). A CO$_2$ laser machine (LS-1416, Boss laser) was used to make a dog bone–like or cylindrical-shaped polymethyl methacrylate (PMMA) plate with 10 mm/s cutting speed and 50% laser power. The PMMA plate was then used to make a casting mold for polydimethylsiloxane (PDMS, Sylgard 184, Dow). The precursor solution was pipetted into the PDMS molds and cross-linked for 120 s with an exposure distance of 10 cm unless otherwise noted. The cross-linked silk fibroin hydrogels were removed from the mold and named as-prepared hydrogels. Swollen hydrogels were obtained by incubating as-prepared hydrogels in 0.9 wt/vol% sodium chloride saline for 3 d at 4 °C. We measured the weight of swollen hydrogels before (M$_w$) and after (M$_d$) drying overnight in a 60 °C oven. The water content was calculated as (M$_w$-M$_d$)/M$_w$ × 100%. Rigid hydrogels were prepared by immersing swollen hydrogels in 90 vol/vol% methanol solution (A412-1, Fisher Chemical) for 1 h, followed by rinsing in 1× PBS for 3 h. Graded hydrogels were made by placing swollen hydrogels on the top of two baths containing water and 90 vol/vol% methanol solution, respectively, for 6 min. Solvent-absorbed tissue paper was used to wrap the ends of the graded hydrogel to minimize solvent evaporation from hydrogels. The β-sheet–induced opacity was imaged and processed to monitor the dynamic process of methanol treatment.

Optical Imaging. Optical images of silk fibroin hydrogels were captured using either digital microscopy (AM7915MZTL, Dino-Lite) or smartphones. Fluorescence images of silk fibroin hydrogels were captured under 300 nm ultraviolet illumination of a transilluminator (FBTI-88, Fisher Scientific). Birefringence images were captured using polarized optical microscopy (Eclipse E200POL, Nikon) equipped with a first-order red retardation plate. The cell-laden hydrogels were imaged in a BZ-X700 microscope (Keyence, IL) for live/dead staining, as well as in a Leica SP8 confocal microscope (Leica Microsystems) for F-actin and the autofluorescence of the silk fibroin. Images were processed using ImageJ (NIH).

Raman Spectroscopy. Raman spectra were obtained using a confocal Raman spectrometer (XploRA plus, Horiba Scientific) equipped with a 785-nm laser (41.8 mW), a 1,200 gr/mm grating, a 50× objective, and a Synapse charge-coupled device (CCD) detector. The confocal hole and the entrance slit were fixed at 500 and 200 μm, respectively. The nominal spectral resolution was 1 cm^{-1}. The Raman spectra were calibrated using a silicon wafer with a characteristic peak at 520 cm^{-1} and were postprocessed via LabSpec 6 software (Horiba Scientific), including averaging, DeNoise smoothing, and baseline subtraction. The Raman spectra were normalized at the peak of 1,615 cm^{-1}, according to previous results (44). The Tyr ratio (I_{850}/I_{830}) is the ratio of the Raman peak at around 850 cm^{-1} to the one at around 830 cm^{-1}. The FWHM was directly measured from the processed Raman spectra.

FTIR Spectroscopy. FTIR spectra were obtained using FTIR-6200 spectroscopy in attenuated total reflection (ATR) mode (Jasco Instruments) equipped with a Diamond/ZnSe crystal (025-2108, PIKE). For each measurement, 64 scans were coadded with a nominal resolution of 4 cm^{-1}. The semiqualitative content of three primary conformations/secondary structures of silk fibroin, including β-sheets, random coils, and β-turns, was analyzed by the spectral deconvolution of the amide I band (1,580 to 1,720 cm^{-1}), according to previous reports (33, 46, 51). Briefly, we subtracted the amide I band with a straight baseline from 1,590 to 1,702 cm^{-1}. The range of Gaussian peaks for each molecular conformation was assigned as follows: 1) β-sheets (1,621 to 1,624 cm^{-1} and 1,698 cm^{-1}), 2) random coils (1,645 to 1,647 cm^{-1}), and 3) β-turns (1,668 cm^{-1}). To remove water interference in the FTIR amide I band, we used lyophilization and deuterium oxide (D_2O) for processing silk fibroin samples. Silk fibroin solutions were lyophilized and directly detected in FTIR spectroscopy; swollen and rigid hydrogels were incubated in 0.9 wt/vol% sodium chloride D_2O solution three times, each for 1 h. The exchange from water to D_2O does not affect the shape and size of silk hydrogels, thus indicating the similar uptake of D_2O as water in hydrogels.

Fluorescence Spectroscopy. Fluorescence spectra were obtained using Hitachi F4500 Spectrofluorometer (Hitachi) and a 10-mm pathlength disposable cuvette (UVette, Eppendorf). The scan rate and wavelength increment were 240 nm/min and 10 nm, respectively. The slits for excitation and emission were 5 and 10 nm, respectively. The voltage of the photomultiplier tube detector was set at 700 V. To increase the fluorescence signal to noise ratio, we lowered the concentration of the precursor solution that consists of 1 wt% silk solution, 0.1 mM Ru(II), and 1 mM SPS.

Rheology. Rheological characterization was performed on an ARES-LS2 rheometer (TA Instruments) equipped with a plain bottom plate of 50 mm diameter and a top transparent plain plate of 20 mm diameter. Oscillatory strain sweep at 1 Hz was performed to obtain linear viscoelastic range (LVR) of precursor silk fibroin solutions. The oscillatory time sweep was performed at 3% strain, within the LVR, and at 1 Hz. For in situ photo–cross-linking, the LED task lamp was placed 10 cm away from the top plate.

Mechanical Characterization. Mechanical characterization was performed using a dynamic mechanical analyzer (RSA3, TA Instruments) equipped with a 35-N loading cell at room temperature. The tensile and compression strain rates were 10 mm/min and 1 mm/min, respectively. Young's modulus was calculated between strains of 0.05 mm/mm and 0.1 mm/mm for tensile tests and between 0.1 mm/mm and 0.15 mm/mm for compression tests. The dimensions of the hydrogel samples were measured by light microscopy before testing. For DMA, a prestain of 5% was applied to hydrogel samples. Oscillatory frequency sweep was performed at 2% strain. The frequency range was limited by the instrument. Elastic resilience was estimated from the damping factor, tan(δ), according to the following equation (10):

$$Resilience\ (\%) = e^{-\frac{1}{2}\pi\tan(\delta)} \times 100. \qquad [1]$$

We adopted the statistical rubber theory to fit the tensile curves, which confirms the rubber-like elasticity. For a swollen rubber-like material with the

effect of chain ends (13, 52), the relationship between stress (σ, Pa) and extension ratio (λ) is expressed as

$$\sigma = \frac{\rho RT}{M_c} v^{\frac{1}{3}}(1 - \frac{2M_c}{M})(\lambda - \frac{1}{\lambda^2}), \qquad [2]$$

where ρ is the silk density (1,421 kg · m^{-3}), R is the molar gas constant (8.3145 Pa · m^3 · K^{-1} · mol^{-1}), T is the temperature (298.15 K), M_c is the average molecular weight between cross-links (kg · mol^{-1} or kDa), M is the nominal molecular weight of regenerated silk fibroin before cross-linking (around 100 kDa in the current work), and v is the polymer fraction (0.25 and 0.14 for as-prepared and swollen hydrogels, respectively). In comparison to classical rubber theory, our model considers the v, as both water and polypeptide chains contribute to the molecular network of the hydrated protein hydrogels.

Cell Encapsulation and In Vitro Degradation. Mouse embryo fibroblasts, C3H/10T1/2s, were purchased from the American Type Culture Collection (ATCC) and maintained in Dulbecco's modified eagle medium (Gibco) with 10% fetal bovine serum and 1% antibiotic-antimycotic solution (Gibco). The 10T1/2 pellets were prepared from the digestion with 0.05% trypsin-ethylenediamine tetraacetic acid (EDTA) and mixed with the precursor solution containing 10 wt% silk fibroin, 1 mM Ru(II), 10 mM SPS, and 0.5 wt% gelatin (porcine skin, Type A, G2500, Sigma-Aldrich) for photo–cross-linking silk hydrogels with a cellular density of 1 million cells/mL. The gelatin was added to promote cell adhesion. The cell-laden silk hydrogels were removed from molds and cultured in the aforementioned conditions. Cell viability and metabolic activity were measured by LIVE/DEAD assays (L3224, Thermo Fisher Scientific) and PrestoBlue HS Cell Viability Reagent (P50200, Thermo Fisher Scientific), respectively. For the PrestoBlue assays, the fluorescence (excitation 560 and emission 590 nm) of culture media was read by a microtiter plate reader (SpectraMax M2, Molecular Devices). To stain the F-actin cytoskeleton, we fixed cell-laden hydrogels in 4% paraformaldehyde PBS solution for 20 min, followed by permeabilization in 0.1% Triton X-100 in PBS for 15 min and incubation in 1:100 solution of Alexa Fluor 488 Phalloidin (A12379, Thermo Fisher Scientific) for 1 h. In vitro enzymatic degradation of swollen silk fibroin hydrogels was performed in 1× PBS solution containing 0.1 U/mL Pronase E (P8811, Sigma-Aldrich) at 37 °C overnight.

Modeling and Simulation. We used COMSOL Multiphysics 5.4 to develop a finite element analysis-based model of dog bone–shaped swollen and graded hydrogels, according to actual size and experimentally obtained Young's moduli. The model of graded hydrogels contains only resilient and rigid regions, while the middle transition region is omitted for model simplification. Young's moduli of 55.5 kPa and 732.1 kPa were assigned to the resilient and rigid regions of the graded hydrogel model, respectively.

Statistical Analysis. Microsoft Excel software was used for all statistical analyses. Statistical comparison among multiple groups was performed using the single-factor ANOVA method, followed by Scheffé's post hoc test. A P value larger than 0.1 was recognized as not statistically significant (n.s.). Unless otherwise described in the text, all experiments were repeated as $n = 3$ independent samples or measurements, and the experimental data were expressed as means $\pm$ SD (s.d.).

Data Availability. All study data are included in the article and/or supporting information.

1. J. Gosline et al., Elastic proteins: Biological roles and mechanical properties. *Philos. Trans. R. Soc. Lond. B Biol. Sci.* **357**, 121–132 (2002).
2. S. Rauscher, R. Pomès, "Structural disorder and protein elasticity" in *Fuzziness: Structural Disorder in Protein Complexes*, M. Fuxreiter, P. Tompa, Eds. (Springer US, New York, NY, 2012), pp. 159–183.
3. N. Annabi et al., Engineering a highly elastic human protein-based sealant for surgical applications. *Sci. Transl. Med.* **9**, eaai7466 (2017).
4. S. Lv et al., Designed biomaterials to mimic the mechanical properties of muscles. *Nature* **465**, 69–73 (2010).
5. G. Chen et al., Plasticizing silk protein for on-skin stretchable electrodes. *Adv. Mater.* **30**, e1800129 (2018).
6. D.-H. Kim et al., Dissolvable films of silk fibroin for ultrathin conformal bio-integrated electronics. *Nat. Mater.* **9**, 511–517 (2010).
7. L. R. Khoury, M. Slawinski, D. R. Collison, I. Popa, Cation-induced shape programming and morphing in protein-based hydrogels. *Sci. Adv.* **6**, eaba6112 (2020).
8. M. Baumgartner et al., Resilient yet entirely degradable gelatin-based biogels for soft robots and electronics. *Nat. Mater.* **19**, 1102–1109 (2020).
9. A. Pena-Francesch, H. Jung, M. C. Demirel, M. Sitti, Biosynthetic self-healing materials for soft machines. *Nat. Mater.* **19**, 1230–1235 (2020).
10. J. M. Gosline, "The structural origin of elasticity and strength" in *Mechanical Design of Structural Materials in Animals* (Princeton University Press, 2018), pp. 59–73, 290–313.

ENGINEERING

BIOCHEMISTRY

Mu et al.
Conformation-driven strategy for resilient and functional protein materials

PNAS | 7 of 8
https://doi.org/10.1073/pnas.2115523119

11. L. D. Muiznieks, F. W. Keeley, Biomechanical design of elastic protein biomaterials: A balance of protein structure and conformational disorder. *ACS Biomater. Sci. Eng.* **3**, 661–679 (2017).

12. R. L. DiMarco, S. C. Heilshorn, Multifunctional materials through modular protein engineering. *Adv. Mater.* **24**, 3923–3940 (2012).

13. C. M. Elvin *et al.*, Synthesis and properties of crosslinked recombinant pro-resilin. *Nature* **437**, 999–1002 (2005).

14. P.-S. Huang, S. E. Boyken, D. Baker, The coming of age of *de novo* protein design. *Nature* **537**, 320–327 (2016).

15. R. Divine *et al.*, Designed proteins assemble antibodies into modular nanocages. *Science* **372**, eabd9994 (2021).

16. T. R. Blum *et al.*, Phage-assisted evolution of botulinum neurotoxin proteases with reprogrammed specificity. *Science* **371**, 803–810 (2021).

17. L. R. Khoury, J. Nowitzke, K. Shmilovich, I. Popa, Study of biomechanical properties of protein-based hydrogels using force-clamp rheometry. *Macromolecules* **51**, 1441–1452 (2018).

18. J. Fang *et al.*, Forced protein unfolding leads to highly elastic and tough protein hydrogels. *Nat. Commun.* **4**, 2974 (2013).

19. B. P. Partlow *et al.*, Highly tunable elastomeric silk biomaterials. *Adv. Funct. Mater.* **24**, 4615–4624 (2014).

20. N. R. Raia *et al.*, Enzymatically crosslinked silk-hyaluronic acid hydrogels. *Biomaterials* **131**, 58–67 (2017).

21. S. Kim *et al.*, All-water-based electron-beam lithography using silk as a resist. *Nat. Nanotechnol.* **9**, 306–310 (2014).

22. D. Ding *et al.*, From soft self-healing gels to stiff films in suckerin-based materials through modulation of crosslink density and β-sheet content. *Adv. Mater.* **27**, 3953–3961 (2015).

23. N. Johari, L. Moroni, A. Samadikuchaksaraei, Tuning the conformation and mechanical properties of silk fibroin hydrogels. *Eur. Polym. J.* **134**, 109842 (2020).

24. E. G. Bellomo, M. D. Wyrsta, L. Pakstis, D. J. Pochan, T. J. Deming, Stimuli-responsive polypeptide vesicles by conformation-specific assembly. *Nat. Mater.* **3**, 244–248 (2004).

25. J. D. Ehrick *et al.*, Genetically engineered protein in hydrogels tailors stimuli-responsive characteristics. *Nat. Mater.* **4**, 298–302 (2005).

26. L. Cera *et al.*, A bioinspired and hierarchically structured shape-memory material. *Nat. Mater.* **20**, 242–249 (2021).

27. A. Miserez, S. S. Wasko, C. F. Carpenter, J. H. Waite, Non-entropic and reversible long-range deformation of an encapsulating bioelastomer. *Nat. Mater.* **8**, 910–916 (2009).

28. A. S. Tatham, P. R. Shewry, Comparative structures and properties of elastic proteins. *Philos. Trans. R. Soc. Lond. B Biol. Sci.* **357**, 229–234 (2002).

29. K. M. Nairn *et al.*, A synthetic resilin is largely unstructured. *Biophys. J.* **95**, 3358–3365 (2008).

30. V. N. Uversky, Intrinsically disordered proteins and their "mysterious" (meta) physics. *Front. Phys.* **7**, 10 (2019).

31. R. Balu, N. K. Dutta, A. K. Dutta, N. R. Choudhury, Resilin-mimetics as a smart biomaterial platform for biomedical applications. *Nat. Commun.* **12**, 149 (2021).

32. X. Mu, V. Fitzpatrick, D. L. Kaplan, From silk spinning to 3D printing: Polymer manufacturing using directed hierarchical molecular assembly. *Adv. Healthc. Mater.* **9**, e1901552 (2020).

33. X. Mu *et al.*, 3D printing of silk protein structures by aqueous solvent-directed molecular assembly. *Macromol. Biosci.* **20**, e1900191 (2020).

34. J. Adamcik, R. Mezzenga, Amyloid polymorphism in the protein folding and aggregation energy landscape. *Angew. Chem. Int. Ed. Engl.* **57**, 8370–8382 (2018).

35. M. J. Harrington, P. Fratzl, Natural load-bearing protein materials. *Prog. Mater. Sci.* **120**, 100767 (2020).

36. M. Tsukada *et al.*, Structural changes of silk fibroin membranes induced by immersion in methanol aqueous solutions. *J. Polym. Sci. B Polym. Phys.* **32**, 961–968 (1994).

37. B. Li, D. O. Alonso, B. J. Bennion, V. Daggett, Hydrophobic hydration is an important source of elasticity in elastin-based biopolymers. *J. Am. Chem. Soc.* **123**, 11991–11998 (2001).

38. S. Rauscher, S. Baud, M. Miao, F. W. Keeley, R. Pomès, Proline and glycine control protein self-organization into elastomeric or amyloid fibrils. *Structure* **14**, 1667–1676 (2006).

39. D. A. Fancy, T. Kodadek, Chemistry for the analysis of protein-protein interactions: Rapid and efficient cross-linking triggered by long wavelength light. *Proc. Natl. Acad. Sci. U.S.A.* **96**, 6020–6024 (1999).

40. X. Mu, J. K. Sahoo, P. Cebe, D. L. Kaplan, Photo-crosslinked silk fibroin for 3D printing. *Polymers (Basel)* **12**, 2936 (2020).

41. K. S. Lim *et al.*, New visible-light photoinitiating system for improved print fidelity in gelatin-based bioinks. *ACS Biomater. Sci. Eng.* **2**, 1752–1762 (2016).

42. A. Martel *et al.*, Silk fiber assembly studied by synchrotron radiation SAXS/WAXS and Raman spectroscopy. *J. Am. Chem. Soc.* **130**, 17070–17074 (2008).

43. M.-E. Rousseau, T. Lefèvre, L. Beaulieu, T. Asakura, M. Pézolet, Study of protein conformation and orientation in silkworm and spider silk fibers using Raman microspectroscopy. *Biomacromolecules* **5**, 2247–2257 (2004).

44. G. Zhou, Z. Shao, D. P. Knight, J. Yan, X. Chen, Silk fibers extruded artificially from aqueous solutions of regenerated Bombyx mori silk fibroin are tougher than their natural counterparts. *Adv. Mater.* **21**, 366–370 (2009).

45. B. Hernández, Y. M. Coïc, F. Pflüger, S. G. Kruglik, M. Ghomi, All characteristic Raman markers of tyrosine and tyrosinate originate from phenol ring fundamental vibrations. *J. Raman Spectrosc.* **47**, 210–220 (2016).

46. X. Hu, D. Kaplan, P. Cebe, Determining beta-sheet crystallinity in fibrous proteins by thermal analysis and infrared spectroscopy. *Macromolecules* **39**, 6161–6170 (2006).

47. Z. Liu, M. A. Meyers, Z. Zhang, R. O. Ritchie, Functional gradients and heterogeneities in biological materials: Design principles, functions, and bioinspired applications. *Prog. Mater. Sci.* **88**, 467–498 (2017).

48. S. Suresh, Graded materials for resistance to contact deformation and damage. *Science* **292**, 2447–2451 (2001).

49. Q. Wang, Q. Chen, Y. Yang, Z. Shao, Effect of various dissolution systems on the molecular weight of regenerated silk fibroin. *Biomacromolecules* **14**, 285–289 (2013).

50. L. S. Wray *et al.*, Effect of processing on silk-based biomaterials: Reproducibility and biocompatibility. *J. Biomed. Mater. Res. B Appl. Biomater.* **99**, 89–101 (2011).

51. C. Guo *et al.*, Thermoplastic moulding of regenerated silk. *Nat. Mater.* **19**, 102–108 (2020).

52. B. Aaron, J. Gosline, Elastin as a random-network elastomer: A mechanical and optical analysis of single elastin fibers. *Biopolymers* **20**, 1247–1260 (1981).